Inorganic Chemistry

pubs.acs.org/IC
Article

Ruddlesden–Popper Oxyfluorides $La_2Ni_{1-x}Cu_xO_3F_2$ ($0 \le x \le 1$): Impact of the Ni/Cu Ratio on the Structure

Jonas Jacobs,* Hai-Chen Wang, Miguel A. L. Marques, Ke Xu, Jörn Schmedt auf der Günne, and Stefan G. Ebbinghaus

Cite This: *Inorg. Chem.* 2024, 63, 6075–6081

ABSTRACT: Ruddlesden–Popper oxyfluorides $La_2Ni_{1-x}Cu_xO_3F_2$ ($0 \le x \le 1$) were obtained by topochemical reaction of oxide precursors $La_2Ni_{1-x}Cu_xO_4$, prepared by citrate-based soft chemistry synthesis, with polyvinylidene fluoride (PVDF) as the fluorine source. Systematic changes of the crystal structure in the oxide as well as the oxyfluoride substitution series were investigated. For $0.2 \le x \le 0.9$, the oxyfluorides adopt the monoclinic ($C2/c$) structural distortion previously solved for the $x = 0.8$ compound based on neutron powder diffraction data, whereas the sample with a lower Cu content of $x = 0.1$ crystallizes in the orthorhombic ($Cccm$) structure variant of $La_2NiO_3F_2$. The orthorhombic-to-monoclinic structural transition was found to be the result of an additional tilt component of the Jahn–Teller elongated CuO_4F_2 octahedra. The structural transitions were additionally studied by DFT calculations, confirming the monoclinic space group symmetry. The "channel-like" anionic ordering of the endmembers $La_2NiO_3F_2$ and $La_2CuO_3F_2$ was checked by ^{19}F MAS NMR experiments and was found to persist throughout the entire substitution series.

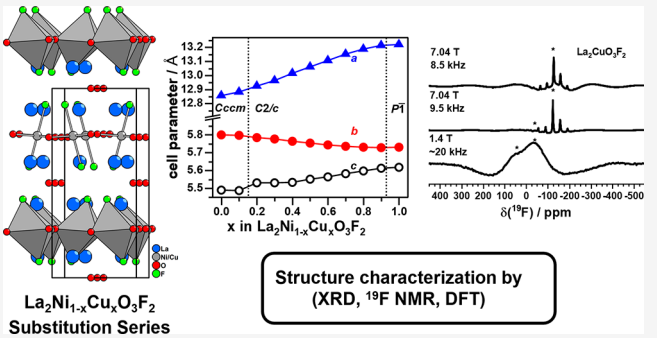

INTRODUCTION

Ruddlesden–Popper (RP) oxides have emerged as a focal point of research in the field of advanced materials due to their intriguing structural properties and potential applications in areas such as energy storage,[1,2] catalysis,[3,4] and electronics.[5,6] Ruddlesden–Popper compounds are characterized by a layered crystal structure (often written as $(AX)(ABX_3)_n$), which distinguishes them from traditional perovskites (ABX_3). The arrangement of perovskite layers with thickness n alternating with one halite-type (AX) layer in the RP structures results in distinctive electronic, magnetic, and optical properties, making them interesting for both fundamental research and industrial applications. Ruddlesden–Popper cuprates A_2CuO_4 are highly prominent representatives for the $n = 1$ member (K_2NiF_4 structure type) of the series due to the first discovery of nonmetal superconductivity in $La_{2-x}Ba_xCuO_{4-y}$ by Bednorz et al.[7] Anionic substitution is widely used to obtain mixed ionic RP compounds with strongly altered structural distortions, which inflict the physical properties. One particular class of materials are the oxyfluorides, of which an increasing number of compounds with different O/F compositions are known to date. These oxyfluorides range from compounds with small fluoride excess like superconducting $La_2CuO_4F_\delta$ ($0 < \delta < 0.25$)[8−10] over stoichiometric compounds with O + F = 4 like Sr_2FeO_3F[11] to highly fluorinated compounds with O + F > 4 (e.g., $LaSrMnO_4F_1$,[12] $La_2CoO_4F_{1.2}$,[2] $Ba_2ZrO_3F_2$,[13] and $Ba_2SnO_{2.5}F_3$[14]). Different low-temperature fluorination methods like the solvothermal reaction with XeF_2[10] as well as reactions with the fluorine-containing polymers polyvinylidene fluoride (PVDF)[15−17] and polytetrafluoroethylene (PTFE)[18] have emerged in recent years, yielding less oxidative synthesis conditions compared to the reaction with F_2 gas, enabling the synthesis of less redox stable oxyfluorides.

Lately, oxyfluorides $La_2NiO_3F_2$,[19] $La_2Ni_{0.2}Cu_{0.8}O_3F_2$, and $La_2CuO_3F_2$[20] were successfully synthesized by the topochemical fluorination of corresponding oxides with PVDF. These compounds share an unusual structural distortion scheme with of strong octahedral tiltings, which result in the formation of a channel-like arrangement of the interstitial anionic positions within the AX layer.

For oxides La_2NiO_4–La_2CuO_4, the whole solid solution series has been described.[21,22] In this study, we report on the successful synthesis of the corresponding oxyfluorides $La_2Ni_{1-x}Cu_xO_3F_2$ ($0.0 \le x \le 1.0$ with $\Delta x = 0.1$). The samples were obtained through topochemical low-temperature fluorination of reactive oxide precursors prepared by the citrate route with PVDF as a fluorination agent. All oxyfluorides were

Received: January 29, 2024
Revised: March 1, 2024
Accepted: March 6, 2024
Published: March 20, 2024

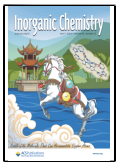

https://doi.org/10.1021/acs.inorgchem.4c00399
Inorg. Chem. 2024, 63, 6075–6081

found to adopt the distorted K_2NiF_4 structure variant found for $La_2NiO_3F_2$ with a transition from orthorhombic ($Cccm$) to monoclinic ($C2/c$) symmetry for $0.2 \leq x \leq 0.9$ due to the Jahn–Teller active Cu^{2+}. The stability of both space groups was investigated by DFT calculations, verifying the structural transition. Additional ^{19}F MAS NMR experiments were applied to check the proposed anion ordering of both endmembers (i.e. $x = 0$ and 1) as well as two of the Ni/Cu-substituted compounds (i.e. $x = 0.3$ and 0.7).

EXPERIMENTAL SECTION

Synthesis. Precursor oxides $La_2Ni_{1-x}Cu_xO_4$ were synthesized in steps of $x = 0.1$ by a citric acid-assisted combustion method.[23] Stoichiometric amounts of La_2O_3 (Merck) (dried at 900 °C for 10 h), Ni powder (Sigma-Aldrich), and copper(II) acetate (98%; Sigma-Aldrich) were dissolved in approximately 25 mL of distilled water with the addition of a few drops of concentrated HNO_3. Citric acid (molar ratio metal ions:citric acid = 1:3) was added while stirring. The obtained clear solutions were subsequently dried on a hot plate at 100 °C until gel formation. The gels were further heated at 350 °C until ignition. The resulting powders were calcinated at 950 °C for 6 h. Oxyfluorides $La_2Ni_{1-x}Cu_xO_3F_2$ were synthesized from the precursor oxides by mixing with polyvinylidene fluoride powder ($PVDF/(CH_2CF_2)_n$) (Alfa Aesar) in a molar ratio of 1:1 (oxide:CH_2CF_2) with a small excess (5%) of the polymer. The mixtures were slowly heated 2 K/min to 350 °C, kept at this temperature for 48 h, and afterward allowed to cool down to room temperature in the box furnace.

Characterization. X-ray diffraction (XRD) patterns were recorded with Cu-$K_{\alpha1,2}$ radiation on a Bragg–Brentano Bruker D8-Advance diffractometer equipped with a 1D silicon strip detector (LynXeye). Patterns were recorded in the angular range of $2\theta = 10–140°$ with a step size of 0.01° and 3 s per step. Additionally, a STOE STADI-MP transmission geometry diffractometer operating with monochromatic Mo-$K_{\alpha1}$ radiation and equipped with a DECTRIS MYTHEN 1K detector was used to record patterns in the angular range of $2\theta = 5–75°$.

For Rietveld refinements, GSAS II[24] was used. The instrumental resolution parameters were obtained from a LaB_6 (STOE STADI-MP) or Al_2O_3 (Bruker D8) reference diffractogram.

The samples were checked for residual polymer by ATR-FT infrared spectroscopy in the range of 4000–250 cm^{-1} with a Bruker Tensor 27 spectrometer.

The La, Ni, and Cu contents of the samples were quantified by X-ray fluorescence spectroscopy (XRF) with a Panalytical Epsilon 4 spectrometer. Data analysis was carried out based on the fundamental parameter approach for pelletized powder samples.

Iodometric titration was used for the determination of the average Ni/Cu oxidation states. About 35 mg of the samples was dissolved in concentrated HCl containing KI in excess. Afterward, 1 g of $NaHCO_3$ was added to create a CO_2-saturated atmosphere, preventing the solutions from autoxidation. For titration, a 0.005 M $Na_2S_2O_3$ solution was used. The obtained oxidation state was calculated from three averaged titrations per sample.

DFT calculations were performed using the projector augmented wave (PAW) setups[25,26] as implemented in the Vienna ab initio simulation (VASP V5.4.) package. For structural optimization, uniform Γ-centered k-point grids with a density of 2000 k-points per reciprocal atom were used to sample the Brillouin zones. For calculations of energy differences between magnetic orderings, denser k-grids with a density of 5 k-points/$Å^{-1}$ were applied. A 520 eV cutoff for the plane-wave basis was used, and the total energies were converged to less than 0.01 meV/cell. The Perdew–Burke–Ernzerhof[27] exchange-correlation functional was used with an on-site 6.2 eV repulsive U correction for Ni 3d states. For the compositions containing both Ni and Cu, different magnetic and structural configurations were generated using the cluster expansion method as implemented in the ATAT package.[28]

^{19}F magic angle spinning (MAS) NMR experiments were performed on a 7.04 T magnet and a 1.4 T magnet operated with an Avance II Bruker NMR console with Topspin V2.1pl8, operating at frequencies of 286 and 56.4 MHz, respectively. Magic angle sample spinning on the 7.04 T magnet was carried out with a homemade MAS probe head for cylindrical rotors with 4 mm outer diameter spinning at around 8.5 to 10 kHz. The samples were packed in 3D-printed inserts made of polypropylene and using a 3D-printed stator.[29] Magic angle sample spinning on the 1.4 T magnet was carried out with a homemade conical stator with the sample packed in 3D-printed conical rotors, spinning at approximately 20 kHz.[30] The chemical shift values refer to neat $CFCl_3$.[31] The spectrum was analyzed with deconv2Dxy.[32]

RESULTS AND DISCUSSION

Crystal Structure Evaluation of Oxides $La_2Ni_{1-x}Cu_xO_4$. The oxyfluoride $La_2NiO_3F_2$ was previously prepared by topochemical fluorination of La_2NiO_4 obtained from solid-state synthesis with La_2O_3 and NiO as starting materials.[19] Our own first experiments showed that a successful formation of the desired Cu-containing oxyfluorides was not possible using this approach. Instead, mixtures of the targeted oxyfluorides, LaOF, and unreacted oxides were usually obtained as products.

The use of more reactive precursor oxides obtained by the citrate-based route at lower calcination temperatures has been successful in the synthesis of $La_2CuO_3F_2$[20] as well as $La_2NiO_{2.5}F_3$.[33] Therefore, this approach was used for the precursor oxides in this work. Phase-pure samples of the whole oxide substitution series $La_2Ni_{1-x}Cu_xO_4$ ($\Delta x = 0.1$) were successfully obtained, and their XRD patterns are shown in Figure 1. For substitution levels of $x \leq 0.4$, an orthorhombic unit cell ($Fmmm$) is indicated by broadening of some peaks with mainly ($hk0$) contribution like the (110) reflection (with respect to the tetragonal ($I4/mmm$) K_2NiF_4 unit cell). For the range of $0.5 \leq x \leq 0.7$, no such broadening is observed and the compounds possess the tetragonal $I4/mmm$ unit cell

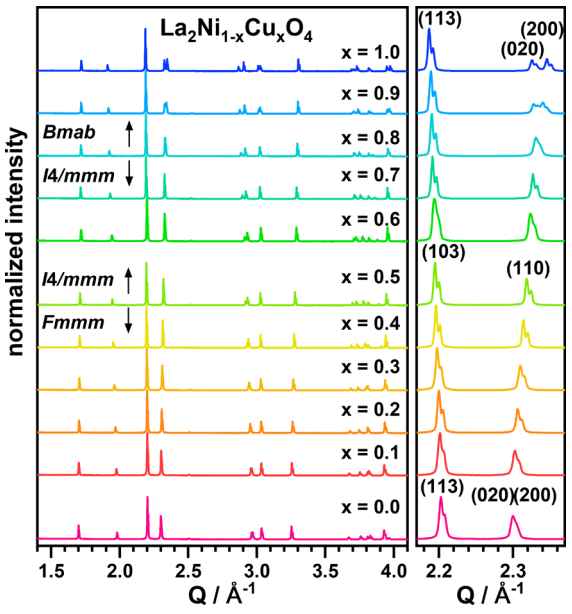

Figure 1. XRD patterns of $La_2Ni_{1-x}Cu_xO_4$ with an enlarged view of the (103)/(110) main reflections (with respect to the $I4/mmm$ K_2NiF_4 structure) highlighting the splitting of (110) into (200)/(020) for $x < 0.5$, and $x > 0.7$ due to the orthorhombic unit cell symmetry.

https://doi.org/10.1021/acs.inorgchem.4c00399
Inorg. Chem. 2024, 63, 6075–6081

symmetry. For copper contents of $x \geq 0.7$, again, a clear splitting of the (110) reflection into two separated reflections ((200)/(020)) indicates a transition from the tetragonal (*I*4/*mmm*) to orthorhombic distorted *B*-centered (*Bmab*) unit cell of La_2CuO_4. Such phase transitions were previously found by Aguadero et al.[22] for oxides which were pepared via classical solid-state synthesis with copper contents of x = 0.0, 0.2, 0.4, 0.6, and 1. Boehm et al.[21] reported slightly different structural behavior with an orthorhombic (*Fmmm*)-to-orthorhombic (*Bmab*) transition at $x > 0.75$ but without the presence of a tetragonal structure throughout the substitution series. The structural transitions observed in this work are therefore in good agreement with the already published data yet provide more details because smaller increments of x have been used.

Rietveld refinements were applied to study the structural evolution and to obtain unit cell parameters for all samples. The Rietveld plots and all crystallographic parameters are shown in the Supporting Information (Table S1 and Figures S1 and S2). The obtained unit cell parameters are plotted in Figure 2a,b, depending on the Cu content x. The increase in unit cell volume is not linear due to an opposed change in parameters a and c. While c increases almost linearly with x throughout the whole substitution series, the parameters a and b decrease with a slightly different slope up to the orthorhombic-to-tetragonal transition at $x \geq 0.4$. Parameters a and b are the same for the compounds with $0.5 \leq x \leq 0.7$ due to the tetragonal unit cell symmetry, and they decrease further with a similar slope as before. Above $x \geq 0.8$, the cell parameter a further decreases, while b even slightly increases, resulting in a stronger increase in the cell volume.

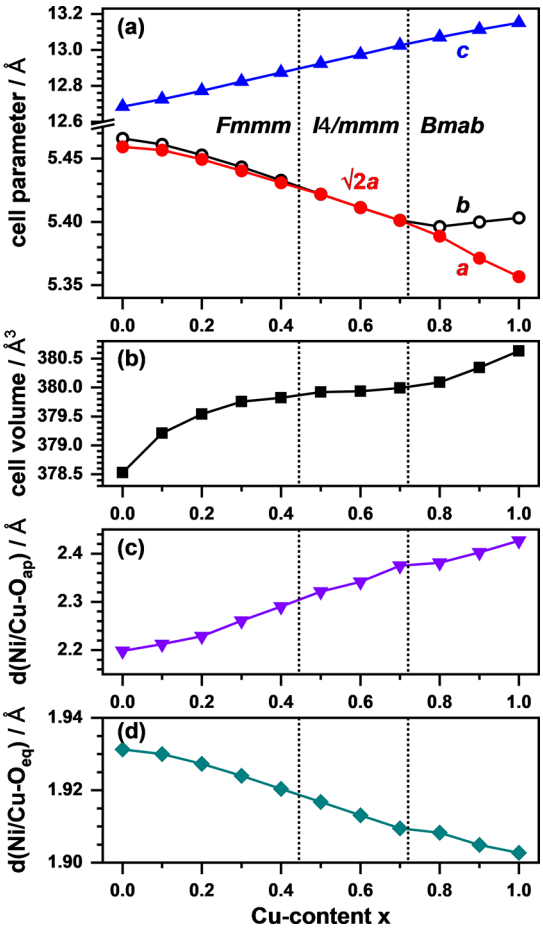

Figure 2. Evolution of the unit cell parameters *a*, *b*, and *c* (a) and cell volume (b) as well as the apical (Ni/Cu−O_{ap}) and equatorial (Ni/Cu−O_{eq}) distances (c, d) with the copper content (x) obtained by Rietveld refinements. The cell parameter *a* is given as $\sqrt{2}a$ for *I*4/*mmm* to achieve comparability between the different centered lattices (*Fmmm*, *I*4/*mmm*, and *Bmab*).

The overall increase in the unit cell volume is interpreted as the result of an increasing Jahn−Teller distortion of the Ni/CuO_6 octahedra with x. For Ni^{2+} ($3d^8$ configuration), no Jahn−Teller distortion is to be expected, while for La_2CuO_4, a strong elongation of the octahedra occurs[34,35] due to the $3d^9$ electron configuration of Cu^{2+}. This increasing octahedral distortion is reflected by a strong and almost linear increase in the apical atomic distance d(Ni/Cu−O_{ap}) from 2.2 to 2.4 Å (x = 0.0 to x = 1.0) accompanied by a less pronounced decrease in the equatorial atomic distance d(Ni/Cu−O_{eq}) from 1.93 to 1.90 Å as plotted in Figure 2c,d, respectively.

Structural and Compositional Characterization of Oxyfluorides $La_2Ni_{1-x}Cu_xO_3F_2$. Fluorination of the precursor oxides was carried out with PVDF in the molar ratio of oxide/CH_2CF_2 (PVDF) of 1:1. Optimized reaction conditions were established by *in situ* XRD experiments published before for the Cu-rich compounds with x = 0.8 and 1.0.[20] As a result, long dwell times of ∼48 h at a comparatively low reaction temperature of 350 °C were found to give the best results. These optimizations were especially needed for the compounds with higher Cu content, as the thermal stability of the fluorinated phase was found to decrease with increasing Cu content. The corresponding oxyfluorides with the formula $La_2Ni_{1-x}Cu_xO_3F_2$ were obtained phase-pure for the entire range of $0 \leq x \leq 1$. The absence of any residual PVDF or other organic phases was confirmed by IR spectroscopy (shown in Figure S3) of the final products. The La:Ni:Cu ratio of both the starting oxides and oxyfluorides was analyzed by XRF measurements. The La:($Ni_{1-x}Cu_x$) ratio was found to be in the range of (1.9−2.1):1, i.e., very close to the expected value, and no major deviations of the nominal nickel/copper ratio were observed. The anionic stoichiometry (3O + 2F) has been verified for both endmembers (x = 0.0 and 1.0) lately,[19,20] and it was also derived from the site occupation factors for the sample with x = 0.8 based on neutron powder diffraction data.[20] As a further support, iodometric titration was applied to determine the bulk oxidation state of nickel/copper in the newly synthesized oxyfluorides. Titration was performed for selected samples (x = 0.2, 0.4, 0.6, and 0.8), and the average oxidation state of the B-type cation was found to be near +2 for both the oxides and oxyfluorides without any systematic dependence on the increasing Cu content. These results demonstrate the non-oxidative[36] nature of fluorination with PVDF and additionally confirm the O_3F_2 anion stoichiometry under the assumption of 5 anions per formula.

The XRD patterns of the $La_2Ni_{1-x}Cu_xO_3F_2$ oxyfluorides are shown in Figure 3. The overall diffraction patterns for $x \leq 0.3$ resemble the one of $La_2NiO_3F_2$, even though a significant decrease in the orthorhombic distortion of the unit cell is indicated by a decrease in the (020)(002) splitting. For $x \geq 0.4$, an additional gradually increasing splitting of the (311) main reflection is observed with increasing x, indicating a transition of the orthorhombic structure of $La_2NiO_3F_2$ (*Cccm*)[19] to the monoclinic unit cell of $La_2Ni_{0.2}CuO_3F_2$ with *C*2/*c* symmetry[20] (see Figure S4 for the symmetry relations of *Cccm* and *C*2/*c*). For $La_2CuO_3F_2$ (x = 1), we previously

https://doi.org/10.1021/acs.inorgchem.4c00399
Inorg. Chem. 2024, 63, 6075−6081

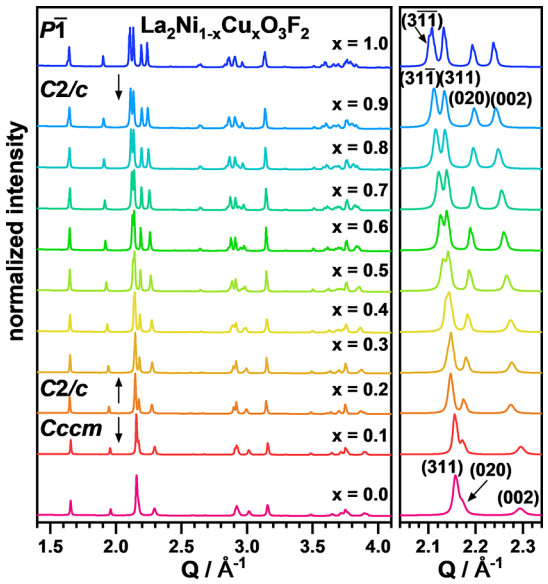

Figure 3. XRD patterns of the oxyfluoride solid solution $La_2Ni_{1-x}Cu_xO_3F_2$ with a detailed view of the main reflections (311) and (020)(002), highlighting the position shifts and changing peak splits.

reported additional symmetry lowering to a triclinic structure (*P*-1), which is for example indicated by a shoulder found at the (31-1) reflection (marked with an arrow in Figure 3) arising from the triclinic cell metric.

Rietveld refinements were conducted as joint refinements based on two X-ray diffraction data sets recorded with monochromatic Mo-$K_{\alpha 1}$ radiation and Cu-$K_{\alpha 1,2}$ radiation. This approach was used to achieve higher redundancy and to combine the advantages of the absence of Ni fluorescence in the Mo-$K_{\alpha 1}$ diffraction patterns and their higher accessible *Q*-range with the better angular resolution of the diffraction patterns taken with Cu radiation. In our previous refinements of the x = 0.8 compound, a split apical octahedral (X_{ap}) position was derived from the refinement of NPD data and this finding was interpreted as the result of a Jahn−Teller distortion of the CuO_4F_2 octahedra in contrast to NiO_4F_2.[20] This split position was not considered in the current refinements because the O/F positions cannot be determined with the required accuracy from XRD data, especially not in the presence of heavy scattering atoms like La/Ni/Cu. Rietveld plots of all refinements and the obtained crystallographic parameters can be found in the Supporting Information (Figures S5 and S6 and Table S2). For x = 0.0 and 0.1, good refinements were achieved with the structural model of $La_2NiO_3F_2$ in the space group *Cccm*. For x = 0.2 to 0.4, an increasing anisotropic broadening of the (311) reflection indicates the transitions from orthorhombic to monoclinic unit cell symmetry and the space group *C*2/*c* was therefore chosen for all compounds with a copper content of $x \geq 0.2$. For x = 0.9, the monoclinic structural model of the x = 0.8 compound and the triclinic structural model of $La_2CuO_3F_2$ were used for the refinements. For both samples, no systematic broadening or splitting of selected reflections was observed even for the highest *Q* values. Therefore, the monoclinic structure model (*C*2/*c*) was chosen. Additional fits in *P*-1 did not yield significantly better residual values despite the larger number of refinable parameters.

The obtained unit cell parameters are plotted in Figure 4a,b. For the longest axis (*a* in *Cccm* and *C*2/*c*), a strong increase is

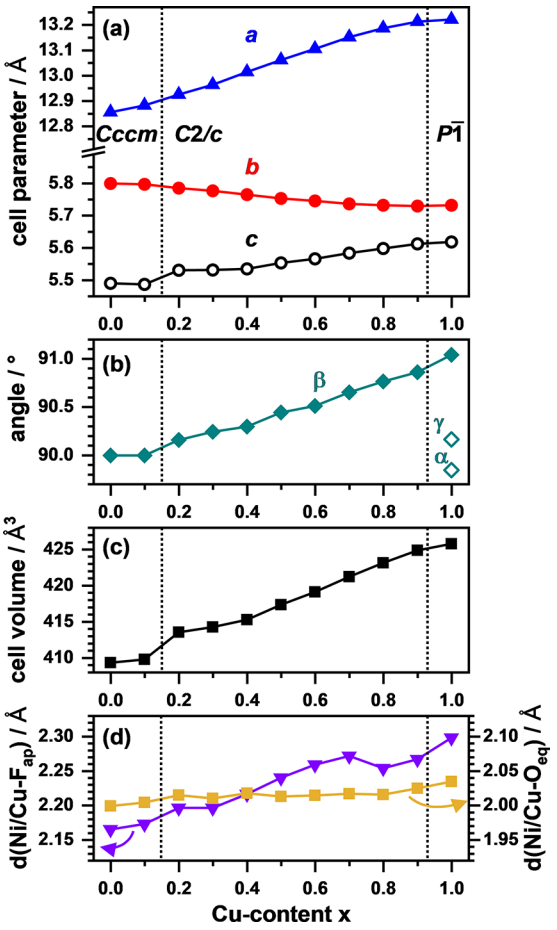

Figure 4. Evolution of the unit cell parameters *a*, *b*, and *c* (a), monoclinic angle β (b), and unit cell volume (c) of $La_2Ni_{1-x}Cu_xO_3F_2$ obtained from Rietveld refinements. In panel (d), the evolution of the Ni/Cu−F_{ap} and Ni/Cu−O_{eq} bond distances is shown.

observed with increasing Cu content ranging from 12.84 Å (x = 0.0) to 13.24 Å (x = 1.0). This is similar to the observations made for the oxides and can be attributed to the higher space requirements of the Jahn−Teller elongated CuO_4F_2 octahedra and the slightly larger ionic radius of Cu^{2+} compared to Ni^{2+} (0.73 Å vs 0.69 Å).[37] For $x \geq 0.7$, a reduction in slope is observed, most probably because the elongation is compensated by the increasing octahedral tilting and, in turn, increased monoclinic distortion as reflected by the increase in the angle β. Additionally, the straining of the *b*/*c* plane becomes smaller as *b* decreases and *c* increases with *x*, again being the result of the altered octahedral tilting scheme with additional tilting component in the *c* direction as found for $La_2Ni_{0.2}Cu_{0.8}O_3F_2$.[20] The cell volume (Figure 4c) increases almost linearly with *x* from 410 to 427 Å^3 despite the observed structural transitions. The Ni/Cu−F_{ap} and Ni/Cu−O_{eq} distances are plotted in Figure 4d, highlighting the impact of substituting Ni^{2+} with the Jahn−Teller active Cu^{2+}. As can be seen, the increase in Ni/Cu−F_{ap} with *x* is less pronounced for the oxyfluorides (2.17 Å − 2.30 Å) compared to the one observed for the precursor oxides shown in Figure 2d. This overall reduction in the Ni/Cu−F_{ap} distance is most probably caused by the additional anion in the halite-type layers, which alters the amounts of La−O/F bonds while keeping the overall bond valence sum of +3, resulting in overall increased La−O/F distances, which in return yield a decreased Ni/Cu−F_{ap} distance.

https://doi.org/10.1021/acs.inorgchem.4c00399
Inorg. Chem. 2024, 63, 6075−6081

The thermodynamic stability of the oxyfluorides crystallizing in space groups *Cccm* and *C*2/*c* depending on the Ni/Cu ratio was additionally studied by DFT calculations. Thirty-two atom unit cells, with increments of $x = 0.25$, were used to simulate all symmetry-inequivalent Ni/Cu occupational configurations as well as magnetic configurations. The relative energies (ΔE) were defined as the difference between the most stable configurations in each phase. The obtained energy difference between *Cccm* and *C*2/*c* can be found in Table 1. The results

Table 1. Energy Difference (ΔE) Obtained from DFT Calculations for Both Unit Cell Symmetries (*Cccm* and *C*2/*c*) with Respect to the Copper Content

copper content (x)	ΔE(*Cccm*-*C*2/*c*) (meV/atom)
0	7.76
0.25	8.75
0.5	10.93
0.75	12.11
1	11.42

show that the monoclinic unit cell is lower in energy and, therefore, more stable for all calculated Ni/Cu ratios even for the pure Ni compound $La_2NiO_3F_2$. This deviation from the experimental results is most probably due to the fact that the energies are calculated for 0 K. Similar results were found by Wissel et al. where the experimental structure of $La_2NiO_3F_2$ relaxes in a monoclinic unit cell after artificial straining.[38] The difference in energy between the *Cccm* and *C*2/*c* structures increases with the copper content, which is also reflected by the increasing monoclinic unit cell distortion (i.e. increasing angle β). Based on these findings, the choice of a monoclinic unit cell for the compounds with $x \geq 0.2$ is justified, although a clear splitting of the diffraction peaks is not in all cases observed due to the limitted resolution of the diffractometers used. To answer the question whether the compounds with $x < 0.2$ also crystallize in a monoclinic unit cell, high-resolution synchrotron XRD data would be needed. Additionally, the smaller value of ΔE for $x = 1$ compared to $x = 0.75$ might be seen as a hint to a structural transition in $La_2CuO_3F_2$, which indeed crystallizes in the space group *P*-1 as reported earlier.[20] This additional symmetry lowering was not considered by the DFT calculations.

^{19}F MAS NMR experiments were conducted for both endmembers $La_2NiO_3F_2$ and $La_2CuO_3F_2$ as well as two members of the solid solution ($x = 0.3$ and 0.7) to check the previously reported anion ordering. For example, in the case of $La_2NiO_3F_2$, a single signal at $\delta = -44$ ppm was previously attributed to an apical ordered fluorine atom.[19] One signal with chemical shifts of $\delta = -20$ ppm ($x = 0.3$) and $\delta = -44$ ppm ($x = 0.0$ and 0.7) is also found in our ^{19}F MAS NMR data (see Figure 5a). A possible explanation for the different chemical shifts may be varying La−F interactions due to changes in the chemical environment of fluorine indirectly caused by Ni/Cu substitution and the corresponding Jahn−Teller elongation. The proposed apical F-ordering is in agreement with the previously reported chemical shift values and our observed spectra. Additional NMR data of $La_2CuO_3F_2$ were recorded on two spectrometers with a 7.04 T magnet and a 1.4 T magnet (Figure 5b). The spectra obtained for the $La_2CuO_3F_2$ sample on the 7.04 T NMR spectrometer are dominated by spinning side bands of the most intense peak at −127 ppm. By using a 1.4 T magnet in combination with a

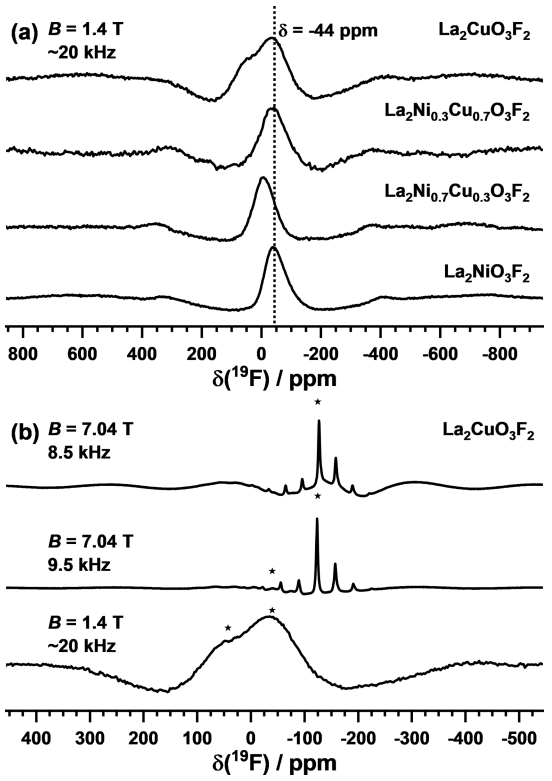

Figure 5. (a) ^{19}F MAS NMR spectra of $La_2NiO_3F_2$, $La_2Ni_{0.7}Cu_{0.3}O_3F_2$, $La_2Ni_{0.3}Cu_{0.7}O_3F_2$, and $La_2CuO_3F_2$ measured in $B = 1.4$ T at the spinning frequency of ca. 20 kHz. (b) ^{19}F MAS NMR spectra of $La_2CuO_3F_2$ measured in 7.04 T at spinning frequencies of 8.5 and 9.5 kHz and in 1.4 T at 20 kHz. The asterisks mark isotropic peaks.

homemade MAS sample holder,[30] the spinning side bands were successfully suppressed through high spinning frequencies of ∼20 kHz, yielding two overlapping and thus not well-resolved peaks for $La_2CuO_3F_2$ centered at 40 and −36 ppm. The peak at −127 ppm of the 7.04 T data is not observed. This signal is attributed to an unknown diamagnetic impurity, which due to the longer relaxation time T_1 of ∼3 s is not observed in the lower field data. This signal is not caused by LaOF for which signals are found at −24 ppm (β-LaOF) or −35 ppm (t-LaOF).[39] The presence of two signals for $La_2CuO_3F_2$ is expected as two crystallographic sites (both with Wyckoff symbol 2*e*) exist for the apical position in the previously reported triclinic structure. As the sites share the same multiplicity, a peak area ratio of 50:50 is expected. This ratio is close to the experimental data, which show a ratio of ∼40:60, given that the broad peaks are not fully resolved. Also, the indication of a slight depopulation of one of the apical octahedral positions is possible, probably due to starting decomposition. This is in accordance with the small amounts of LaOF found in the XRD data of this sample.

CONCLUSIONS

The topochemical fluorination of the solid solution $La_2Ni_{1-x}Cu_xO_4$ was carried out with PVDF as a fluorination agent, yielding phase-pure oxyfluoride samples for the whole substitution series $La_2Ni_{1-x}Cu_xO_3F_2$. The structure of the obtained oxides was studied in increments of $x = 0.1$ by X-ray powder diffraction experiments, and two structural transitions were observed (orthorhombic (*Fmmm*; $x \leq 0.4$) → tetragonal

https://doi.org/10.1021/acs.inorgchem.4c00399
Inorg. Chem. 2024, 63, 6075−6081

($I4/mmm$; $0.4 < x \leq 0.7$) → orthorhombic ($Bmab$; $0.7 < x \leq 1.0$)). For the oxyfluorides, we were able to show that the solid solution exhibits a structural transition at $x = 0.2$ from the orthorhombic structure of $La_2NiO_3F_2$ to the monoclinic distorted structure of $La_2Ni_{0.2}Cu_{0.8}O_3F_2$, which we previously solved based on NPD data,[20] while for $La_2CuO_3F_2$, even further symmetry lowering to $P\text{-}1$ was found. This transition is driven by an increased Jahn−Teller distortion. The structural transition was also studied by DFT calculations, and based on the difference in thermodynamic stability between both space groups, the presence of the monoclinic structure was further confirmed. The previously proposed apical fluoride anion ordering of $La_2NiO_3F_2$ and $La_2CuO_3F_2$ was further verified for $x = 0.0$, 0.3, 0.7, and 1.0 by additional ^{19}F MAS NMR experiments. In this paper, we were therefore able to show the existence of several new oxyfluorides all exhibiting a similar anion ordering scheme and to refine their strucutres. In a follow-up article, we will discuss the impact of Ni/Cu substitution on the thermal stability as well as the magnetic properties of $La_2Ni_{1-x}Cu_xO_3F_2$ as these results would by far exceed the scope of this article.

■ ASSOCIATED CONTENT

Supporting Information

The Supporting Information is available free of charge at https://pubs.acs.org/doi/10.1021/acs.inorgchem.4c00399.

FTIR spectra of $La_2Ni_{1-x}Cu_xO_4$ and $La_2Ni_{1-x}Cu_xO_3F_2$ in comparison to PVDF; Rietveld plots from the refinement of XRD data of $La_2Ni_{1-x}Cu_xO_4$ and $La_2Ni_{1-x}Cu_xO_3F_2$; crystallographic data of $La_2Ni_{1-x}Cu_xO_4$ and $La_2Ni_{1-x}Cu_xO_3F_2$ obtained from Rietveld refinements (PDF)

Accession Codes

CCDC 2329401−2329421 contain the supplementary crystallographic data for this paper. These data can be obtained free of charge via www.ccdc.cam.ac.uk/data_request/cif, or by emailing data_request@ccdc.cam.ac.uk, or by contacting The Cambridge Crystallographic Data Centre, 12 Union Road, Cambridge CB2 1EZ, UK; fax: +44 1223 336033.

■ AUTHOR INFORMATION

Corresponding Author

Jonas Jacobs − *Faculty of Natural Sciences II, Institute of Chemistry, Inorganic Chemistry, Martin Luther University Halle-Wittenberg, Halle D-06120, Germany;* orcid.org/0000-0001-5473-9650; Email: jonas.jacobs@chemie.uni-halle.de

Authors

Hai-Chen Wang − *Research Center Future Energy Materials and Systems of the University Alliance Ruhr, Faculty of Mechanical Engineering, Ruhr University Bochum, Bochum D-44801, Germany;* orcid.org/0000-0002-2892-5879

Miguel A. L. Marques − *Research Center Future Energy Materials and Systems of the University Alliance Ruhr, Faculty of Mechanical Engineering, Ruhr University Bochum, Bochum D-44801, Germany;* orcid.org/0000-0003-0170-8222

Ke Xu − *Faculty IV: School of Science and Technology, Department of Chemistry and Biology, Inorganic Materials Chemistry, University of Siegen, Siegen D-57076, Germany*

Jörn Schmedt auf der Günne − *Faculty IV: School of Science and Technology, Department of Chemistry and Biology, Inorganic Materials Chemistry, University of Siegen, Siegen D-57076, Germany;* orcid.org/0000-0003-2294-796X

Stefan G. Ebbinghaus − *Faculty of Natural Sciences II, Institute of Chemistry, Inorganic Chemistry, Martin Luther University Halle-Wittenberg, Halle D-06120, Germany;* orcid.org/0000-0001-6391-2582

Complete contact information is available at: https://pubs.acs.org/10.1021/acs.inorgchem.4c00399

Author Contributions

J.J.: conceptualization, data curation, formal analysis, investigation, methodology, visualization, and writing of the original draft. H.-C.W. and M.A.L.M.: performing and interpretation of theoretical calculations and review. K.X. and J.S.a.d.G.: collection and analysis of ^{19}F MAS NMR data and review. S.G.E.: project administration, resources, supervision, validation, and review and editing.

Notes

The authors declare no competing financial interest.

■ REFERENCES

(1) Nowroozi, M. A.; Wissel, K.; Rohrer, J.; Munnangi, A. R.; Clemens, O. $LaSrMnO_4$: Reversible Electrochemical Intercalation of Fluoride Ions in the Context of Fluoride Ion Batteries. *Chem. Mater.* **2017**, *29* (8), 3441−3453.

(2) Nowroozi, M. A.; Ivlev, S.; Rohrer, J.; Clemens, O. La_2CoO_4: A New Intercalation Based Cathode Material for Fluoride Ion Batteries with Improved Cycling Stability. *J. Mater. Chem. A* **2018**, *6* (11), 4658−4669.

(3) Huang, Y.; Wei, Y.; Cheng, S.; Fan, L.; Li, Y.; Lin, J.; Wu, J. Photocatalytic Property of Nitrogen-Doped Layered Perovskite $K_2La_2Ti_3O_{10}$. *Sol. Energy Mater. Sol. Cells* **2010**, *94* (5), 761−766.

(4) Zhao, B.; Wang, R.; Yao, W.; Yang, X.; Zhou, B. The Effect of Copper Substitution on $La_2Ni_{1-x}Cu_xO_4$ Catalysts Activity for Simultaneous Removal of NO_x and Diesel Soot. *Catal. Lett.* **2009**, *132* (1−2), 41−49.

(5) Liu, X. Q.; Wu, J. W.; Shi, X. X.; Zhao, H. J.; Zhou, H. Y.; Qiu, R. H.; Zhang, W. Q.; Chen, X. M. Hybrid Improper Ferroelectricity in Ruddlesden-Popper $Ca_3(Ti,Mn)_2O_7$ Ceramics. *Appl. Phys. Lett.* **2015**, *106* (20), 202903.

(6) Zhang, Q.; Solanki, A.; Parida, K.; Giovanni, D.; Li, M.; Jansen, T. L. C.; Pshenichnikov, M. S.; Sum, T. C. Tunable Ferroelectricity in Ruddlesden-Popper Halide Perovskites. *ACS Appl. Mater. Interfaces* **2019**, *11* (14), 13523−13532.

(7) Bednorz, J. G.; Müller, K. A.; Ott, H. R. Possible High T_c Superconductivity in the Ba — La — Cu — O System. *Z. Phys. B-Condensed Matter* **1993**, *64*, 267−271.

(8) Vasala, S.; Alff, L.; Clemens, O. Tuning of Superdiamagnetism in La_2CuO_4 by Solid-State Electrochemical Fluorination and Defluorination. *APL Mater.* **2021**, *9* (4), 41107.

(9) Chen, X.; Tang, K.; Zeng, S.; Hao, Q.; Wang, D.; Gao, Z.; Wang, Y. Fluorination of $La_{2-x}Sr_xCuO_4$ (x = 0, 0.15, 0.3) and Study on the Crystal Structures, Magnetic Properties of Their Fluorinated Products. *J. Alloys Compd.* **2015**, *626*, 239−244.

(10) Abakumov, A. M.; Hadermann, J.; Van Tendeloo, G.; Shpanchenko, R. V.; Oleinikov, P. N.; Antipov, E. V. Anion Ordering in Fluorinated La_2CuO_4. *J. Solid State Chem.* **1999**, *142* (2), 440−450.

(11) Case, G. S.; Hector, A. L.; Levason, W.; Needs, R. L.; Thomas, M. F.; Weller, M. T. Syntheses, Powder Neutron Diffraction Structures and Mossbauer Studies of Some Complex Iron Oxyfluorides: $Sr_3Fe_2O_6F_{0.87}$, Sr_2FeO_3F and $Ba_2InFeO_5F_{0.68}$. *J. Mater. Chem.* **1999**, *9* (11), 2821−2827.

(12) Aikens, L. D.; Li, R. K.; Greaves, C. The Synthesis and Structure of a New Oxide Fluoride, $LaSrMnO_4F$, with Staged Fluorine Insertion. *Chem. Commun.* **2000**, *21*, 2129−2130.
(13) Slater, P. R.; Gover, K. B. Synthesis and Structure of the New Oxide Fluoridea $Ba_2ZrO_3F_2{\cdot}xH_2O$ (x≈0.5). *J. Mater. Chem.* **2001**, *11* (8), 2035−2038.
(14) Berry, F. J.; Moore, E.; Mortimer, M.; Ren, X.; Heap, R.; Slater, P.; Thomas, M. F. Synthesis and Structural Investigation of a New Oxide Fluoride of Composition $Ba_2SnO_{2.5}F_3{\cdot}xH_2O$ (x≈0.5). *J. Solid State Chem.* **2008**, *181* (9), 2185−2190.
(15) Slater, P. R. Poly(Vinylidene Fluoride) as a Reagent for the Synthesis of K_2NiF_4-Related Inorganic Oxide Fluorides. *J. Fluor. Chem.* **2002**, *117* (1), 43−45.
(16) Clemens, O.; Wright, A. J.; Berry, F. J.; Smith, R. I.; Slater, P. R. Synthesis, Structural and Magnetic Characterisation of the Fully Fluorinated Compound 6H-$BaFeO_2F$. *J. Solid State Chem.* **2013**, *198*, 262−269.
(17) Clemens, O.; Kuhn, M.; Haberkorn, R. Synthesis and Characterization of the $La_{1-x}Sr_xFeO_{3-\delta}$ System and the Fluorinated Phases $La_{1-x}Sr_xFeO_{3-x}F_x$. *J. Solid State Chem.* **2011**, *184* (11), 2870−2876.
(18) Tsujimoto, Y.; Yamaura, K.; Hayashi, N.; Kodama, K.; Igawa, N.; Matsushita, Y.; Katsuya, Y.; Shirako, Y.; Akaogi, M.; Takayama-Muromachi, E. Topotactic Synthesis and Crystal Structure of a Highly Fluorinated Ruddlesden-Popper-Type Iron Oxide, $Sr_3Fe_2O_{5+x}F_{2-x}$ (x ≈ 0.44). *Chem. Mater.* **2011**, *23* (16), 3652−3658.
(19) Wissel, K.; Heldt, J.; Groszewicz, P. B.; Dasgupta, S.; Breitzke, H.; Donzelli, M.; Waidha, A. I.; Fortes, A. D.; Rohrer, J.; Slater, P. R.; Buntkowsky, G.; Clemens, O. Topochemical Fluorination of La_2NiO_{4+d}: Unprecedented Ordering of Oxide and Fluoride Ions in $La_2NiO_3F_2$. *Inorg. Chem.* **2018**, *57* (11), 6549−6560.
(20) Jacobs, J.; Hester, J. R.; Ebbinghaus, S. G. Cuprate Oxyfluorides $La_2Cu_{0.8}Ni_{0.2}O_3F_2$ and $La_2CuO_3F_2$ with "Channel-like" Anion Ordering. *Inorg. Chem.* **2022**, *61* (43), 17202−17211.
(21) Boehm, E.; Bassat, J. M.; Steil, M. C.; Dordor, P.; Mauvy, F.; Grenier, J. C. Oxygen Transport Properties of $La_2Ni_{1-x}Cu_xO_{4+\delta}$ Mixed Conducting Oxides. *Solid State Sci.* **2003**, *5* (7), 973−981.
(22) Aguadero, A.; Alonso, J. A.; Escudero, M. J.; Daza, L. Evaluation of the $La_2Ni_{1-x}Cu_xO_{4+\delta}$ System as SOFC Cathode Material with 8YSZ and LSGM as Electrolytes. *Solid State Ionics* **2008**, *179* (11−12), 393−400.
(23) Guo, C.; Zhang, X.; Zhang, J.; Wang, Y. Preparation of La_2NiO_4 Catalyst and Catalytic Performance for Partial Oxidation of Methane. *J. Mol. Catal. A Chem.* **2007**, *269* (1−2), 254−259.
(24) Toby, B. H.; Von Dreele, R. B. GSAS-II: The Genesis of a Modern Open-Source All Purpose Crystallography Software Package. *J. Appl. Crystallogr.* **2013**, *46* (2), 544−549.
(25) Blochl, P. E.; Blöchl, P. E. Projector Augmented-Wave Method. *Phys. Rev. B* **1994**, *50* (24), 17953−17979.
(26) Kresse, G.; Furthmüller, J. Efficiency of Ab-Initio Total Energy Calculations for Metals and Semiconductors Using a Plane-Wave Basis Set. *Comput. Mater. Sci.* **1996**, *6* (1), 15−50.
(27) Perdew, J. P.; Burke, K.; Ernzerhof, M. Generalized Gradient Approximation Made Simple. *Phys. Rev. Lett.* **1996**, *77* (18), 3865−3868.
(28) van de Walle, A. Multicomponent Multisublattice Alloys, Nonconfigurational Entropy and Other Additions to the Alloy Theoretic Automated Toolkit. *Calphad Comput. Coupling Phase Diagrams Thermochem.* **2009**, *33* (2), 266−278.
(29) Xu, K.; Pecher, O.; Braun, M.; Schmedt auf der Günne, J. Stable Magic Angle Spinning with Low-Cost 3D-Printed Parts. *J. Magn. Reson.* **2021**, No. 107096.
(30) Xu, K.; Aldudak, F.; Pecher, O.; Braun, M.; Neuberger, A.; Foysi, H.; Schmedt auf der Günne, J. High Resolution Solid-State NMR on the Desktop. *Solid State Nucl. Magn. Reson.* **2023**, *126* (June). 101884.
(31) Harris, R. K.; Becker, E. D.; Cabral de Menezes, S. M.; Goodfellow, R.; Granger, P. NMR Nomenclature: Nuclear Spin Properties and Conventions for Chemical Shifts - IUPAC Recommendations 2001. *Solid State Nucl. Magn. Reson.* **2002**, *22* (4), 458−483.
(32) Avadhut, Y. S.; Schneider, D.; Schmedt auf der Günne, J. A Method for Improved Quantification of 1H NMR Signals under Low-Resolution Conditions for Solids. *J. Magn. Reson.* **2009**, *201* (1), 1−6.
(33) Jacobs, J.; Marques, M. A. L.; Wang, H. C.; Dieterich, E.; Ebbinghaus, S. G. Structure, Magnetism, and Thermal Stability of $La_2NiO_{2.5}F3$: A Ruddlesden-Popper Oxyfluoride Crystallizing in Space Group $P4_2/nnm$. *Inorg. Chem.* **2021**, *60* (17), 13646−13657.
(34) Grande, B.; Müller-Buschbaum, H. Über Oxocuprate. XVIII. Zur Kenntnis von $Sr_2CuO_2Br_2$ Mit Einem Beitrag Über La_2NiO_4. *Zeitschrift fur Anorg. und Allg. Chemie* **1977**, *433* (1), 152−156.
(35) Müller-Buschbaum, H.; Lehmann, U. Zum Problem Der Oktaederstreckung an La_2CuO_4, La_2NiO_4 Mit Einem Beitrag Über $CaSmAlO_4$. *ZAAC - J. Inorg. Gen. Chem.* **1978**, *447* (1), 47−52.
(36) Clemens, O.; Slater, P. R. Topochemical Modifications of Mixed Metal Oxide Compounds by Low-Temperature Fluorination Routes. *Rev. Inorg. Chem.* **2013**, *33* (2−3), 105−117.
(37) Shannon, R. D. Revised Effective Ionic Radii and Systematic Studies of Interatomic Distances in Halides and Chalcogenides. *Acta Crystallogr., Sect. A* **1976**, *32* (5), 751−767.
(38) Wissel, K.; Malik, A. M.; Vasala, S.; Plana-Ruiz, S.; Kolb, U.; Slater, P. R.; da Silva, I.; Alff, L.; Rohrer, J.; Clemens, O. Topochemical Reduction of $La_2NiO_3F_2$: The First Ni-Based Ruddlesden−Popper n = 1 T′-Type Structure and the Impact of Reduction on Magnetic Ordering. *Chem. Mater.* **2020**, *32* (7), 3160−3179.
(39) Dabachi, J.; Body, M.; Dittmer, J.; Fayon, F.; Legein, C. Structural Refinement of the RT LaOF Phases by Coupling Powder X-Ray Diffraction, ^{19}F and ^{139}La Solid State NMR and DFT Calculations of the NMR Parameters. *Dalt. Trans.* **2015**, *44* (47), 20675−20684.

https://doi.org/10.1021/acs.inorgchem.4c00399
Inorg. Chem. 2024, 63, 6075−6081